Computers and Electronics in Agriculture 158 (2019) 294–302

Contents lists available at ScienceDirect

Computers and Electronics in Agriculture

journal homepage: www.elsevier.com/locate/compag

Original papers

A comparison of object-based image analysis approaches for field boundary delineation using multi-temporal Sentinel-2 imagery

Barry Watkins*, Adriaan van Niekerk

Department of Geography and Environmental Studies, University of Stellenbosch, South Africa

ARTICLE INFO

Keywords:
Crop field boundary delineation
Earth observation
Edge detection
Segmentation
Sentinel-2
Knowledge-based classification

ABSTRACT

In this study we evaluated several Earth observation methodologies for automatically delineating crop field boundaries from multi-temporal Sentinel-2 imagery. The methodology makes use of edge detection that is applied to multiple images acquired during a growing season and image segmentation to delimit agricultural fields, orchards and vineyards. Two edge detection operators (Canny and Scharr) and three image segmentation algorithms (watershed, multi-threshold and multi-resolution) were combined and evaluated, resulting in six experiments (scenarios). A rule-based (knowledge-based) classification was applied to the extracted image objects to discard uncultivated areas. Reference field boundaries, manually digitised from very high (10 cm) resolution aerial imagery, were used for quantitative accuracy assessments and qualitative comparisons. The quantitative accuracy assessment consisted of both area- and edge-based metrics. The results showed that the watershed segmentation, combined with Canny edge detection, produced the most accurate field boundaries with an OA of 92.9% and combined MAE of 24.5 m. The Scharr algorithm produced thicker edges, causing positional errors along the boundaries. The multi-resolution and multi-threshold segmentation algorithms produced boundary inaccuracies ranging from 1 to 3 pixels, largely due to the creation of thick boundary objects, which caused offsets of the extracted borders on both sides of the reference boundaries. The combination of Canny edge detection (performed on multiple Sentinel-2 images acquired during the growing season) and watershed segmentation is thus recommended for operational field boundary delineation.

1. Introduction

The spatial extent and location of agricultural fields is critical for the implementation of precision agriculture, crop yield estimations, food security assessments and resource planning (Alemu, 2016; Johnson, 2013; Yan & Roy, 2014). Agricultural statistics are commonly calculated per-field, and results are negatively affected by inaccurate or outdated field boundaries (Rydberg & Borgefors, 2001; Turker & Kok, 2013). Classifying crops using a per-field (object-based) approach is known to produce better results than a per-pixel method (Blaschke et al., 2014; Peña et al., 2014; Schultz et al., 2015). However despite the advantages of such object-based methods, robust techniques to automatically delineate agricultural field boundaries remains elusive (Belgiu & Csillik, 2018).

A number of remote sensing approaches for determining cropland extent have been explored. Many of these approaches are applied at regional or global scale, using low to medium resolution satellite imagery (Lunetta et al., 2010; Wardlow et al., 2007). Pittman et al. (2010) showed the benefits of using multi-temporal MODIS (250 m spatial resolution) imagery for generating a global cropland probability layer. Roumenina et al. (2015) assessed the crop mapping performance of multi-temporal PROBA-V (100 m spatial resolution) against PROBA-V (300 m spatial resolution) imagery in a test site in Bulgaria. Their findings demonstrated an increase in crop mapping accuracy (by 5.8–14.8%) when the higher (100 m) spatial resolution imagery was used. Gilbertson et al. (2017) showed that pansharpening Landsat-8 imagery from 30 m to 15 m spatial resolution improved crop type classification accuracies by up to 15%, but noted that the use of multi-temporal imagery is critical for achieving good results. From these studies it would seem that both high spatial and high-temporal resolution imagery is required for accurate field boundary delineation (Alemu, 2016; Mueller et al., 2004).

The Copernicus programme is an Earth observation initiative that will provide unprecedented levels of observational capabilities, mainly through the operations of recently launched satellites (called Sentinels). The Sentinel-2 satellite constellation provides a significant increase in observational capacity compared to other satellites such as Landsat, thanks to its large number (13) of spectral bands, high (10–60 m)

* Corresponding author.
E-mail address: barrywatkins94@hotmail.co.za (B. Watkins).

https://doi.org/10.1016/j.compag.2019.02.009
Received 28 November 2018; Received in revised form 5 February 2019; Accepted 9 February 2019
Available online 20 February 2019
0168-1699/

spatial resolutions and short (five-day) revisit times (Lebourgeois et al., 2017). This data allows for more timely estimates of crop area extents, crop types and crop conditions, which are all major indicators of a region's agricultural activity (Bontemps et al., 2015). Although the resolution of Sentinel-2 images is not as high as many commercial very high resolution (VHR) satellites (e.g. WorldView 2 – 4), its short revisit periods, wide spectral range (including narrow red edge bands) and free access hold much potential for operational (automated) field boundary delineation.

Field boundary delineation using remotely sensed imagery can generally be categorised into edge-based and region-based techniques (Rydberg & Borgefors, 1999; Turker & Kok, 2013; Wuest & Zhang, 2009). Edge-based methods focus on detecting the edges (discontinuities between pixel values) in images that are used as candidate pixels for region boundaries. There are a range of edge detectors; from simple algorithms such as the Sobel or Scharr operators, to more complex techniques such as the Canny operator (Shrivakshan & Chandrasekar, 2012). These algorithms rapidly partition images into edges and non-edges. However, boundaries between objects are not always well defined, which can lead to gaps in the boundaries. Furthermore, most edge detectors are sensitive to noise as they often exploit local contrasts, which may lead to errors such as false edges (Chen et al., 2015). These errors require post-processing procedures such as gap-filling, edge-tracking and smoothing in order to create well-defined boundaries (Fan et al., 2001). Rydberg & Borgefors (1999) presented a multispectral edge detection method to delineate agricultural fields using single-date Landsat (30 m) imagery. A gradient edge detector was used to generate the edge magnitude and direction. Weighted addition, based on the edge direction, was applied to enhance edges and reduce noise. The resulting edge image was thinned using edge direction and magnitude, followed by hysteresis thresholding to produce the field boundaries. A qualitative assessment showed accurate field boundary delineation, but the method did not produce closed boundaries. Turker & Kok (2013) devised a method for detecting sub-boundaries by employing Canny edge detection on single-date SPOT4 (20 m) and SPOT5 (10 m) multispectral imagery covering an agricultural area in Turkey. Line segments were created from edge chains, followed by the elimination of spurious line segments through a geometrical simplification process. Lastly, perceptual grouping of the line segments was performed using Gestalt laws. The study reported matching percentages between the reference data and extracted segments of 82.6% and 76.2% for the SPOT5 and SPOT4 images respectively.

In contrast to edge-based methods that exploit variations in the image, region-based methods group pixels into objects based on some homogeneity criterion (Alemu, 2016; Mueller et al., 2004). Multi-resolution segmentation (MRS), as detailed in Baatz & Schäpe (2000), is a popular region-based segmentation algorithm used for field boundary delineation. MRS begins with a set of seed pixels that are iteratively merged according to some heterogeneity/homogeneity criterion (Schultz et al., 2015). Belgiu & Csillik (2018) performed MRS on multi-temporal Sentinel-2 imagery for cropland mapping. Segmentation of crop fields proved difficult as fields with high internal variation were found to be over-segmented, while small adjacent fields were under-segmented. Watershed segmentation (WS), another popular region-based segmentation algorithm, is applied to a single gradient image with the objective of finding regions of high intensity (watersheds) that divide regions of local minima (basins) (Salman, 2006). Butenuth et al. (2004) employed the WS algorithm to delineate agricultural fields from aerial imagery. GIS knowledge of existing field boundaries were used to support the segmentation. The results displayed the potential of the technique to delineate agricultural fields. Multi-threshold segmentation (MTS) is another simple and effective segmentation algorithm that can quickly partition an image based on the image histogram (Carleer et al., 2005). A disadvantage of region-based algorithms is that errors often occur along field boundaries when objects stop growing before the actual boundary is reached (Chen et al., 2015). Field boundaries consequently form a separate region of homogeneity, which can lead to the creation of sliver polygons along field edges. In effect, this causes the extracted field boundary to shift inwards (towards the centre of the field).

A hybrid approach, that integrates both edge-based and region-based methods has been proposed to exploit the advantages of each (Rydberg & Borgefors, 2001). For instance, Mueller et al. (2004) demonstrated the value of object-based image analysis (OBIA) for extracting agricultural fields from very high resolution single-date panchromatic imagery. Edge detection was performed at different spatial resolutions (4.5 m, 5.8 m and 1 m) to detect pertinent edges. This was followed by an edge-guided smoothing and region growing segmentation to produce field boundaries. Similarly, Rydberg & Borgefors (2001) segmented single-date high resolution (20 m SPOT4 and 30 m Landsat-7) multispectral images to delineate agricultural field boundaries. A gradient edge detector was utilised to extract edge images from each band, which were then aggregated using weighted vector addition. The resulting edge image was combined with a segmentation algorithm based on an ISODATA algorithm. The high (87%) overall accuracy (OA) achieved was attributed to the method's ability to exploit edges from several bands. Li et al. (2010) also followed a hybrid approach by employing the WS algorithm on multiple Quickbird images. Edge detection with an embedded confidence measure was first performed to amplify weak edges. This was followed by a marker-based watershed algorithm to delineate the object boundaries. The procedure was reported to provide satisfactory results with little over-segmentation and a boundary accuracy of approximately 78%. In another hybrid approach, Alemu (2016) made use of a line segment detection algorithm to extract linear features on very high resolution (2 m) Worldview-2 imagery. Changes in the x and y directions of each band were combined using a vector sum. A line-support region representing potential candidates for a segment was formed using a region growing technique. Two metrics based on the distance and orientation of boundaries, namely ratio of missing detections (RM) and ratio of false detections (RF), were used to validate the results. The results obtained for RM and RF were 0.78 and 0.73 respectively (where values closer to one represent higher accuracies). However, the accuracy measures did not distinguish between field boundary edges and other edges (e.g. edges formed by tree shadows), thus leading to the false detection of edges and overestimation of RM and RF values. Upon visual inspection of the results, the developed methodology tended to omit many field boundaries, which was attributed to the heterogeneous landscape and weak contrast between neighbouring fields.

One common limitation of the field boundary delineation methods mentioned above is the use of single-date imagery. Finding the edge of a field is challenging when different crop types have similar spectral and structural properties at certain stages of their phenological growth cycle (Esfahani, 2014; Pittman et al., 2010). This is compounded when a single crop is grown on adjacent fields. Therefore, it is necessary to use multiple images throughout the growing season to accurately detect spatial transitions (edges) between different crop types as well as crops of the same type (Inglada et al., 2015). Sentinel-2 imagery (Drusch et al., 2012), available at 10 m spatial resolution and at unprecedentedly short intervals (five-day revisit time), has opened up new possibilities for operational (automated) crop field boundary delineation using Earth observation methods.

The primary aim of this study is to compare and evaluate several OBIA techniques for automatically delineating agricultural field boundaries from multi-temporal Sentinel-2 imagery. Two edge detection and three image segmentation algorithms are configured in different combinations to construct six experiments. The results of the experiments are compared and assessed against reference field boundaries in Vaalharts, the largest irrigation scheme of South Africa. The results of the experiments are interpreted in the context of finding an operational methodology for identifying agricultural field boundaries in complex and dynamic irrigation schemes.

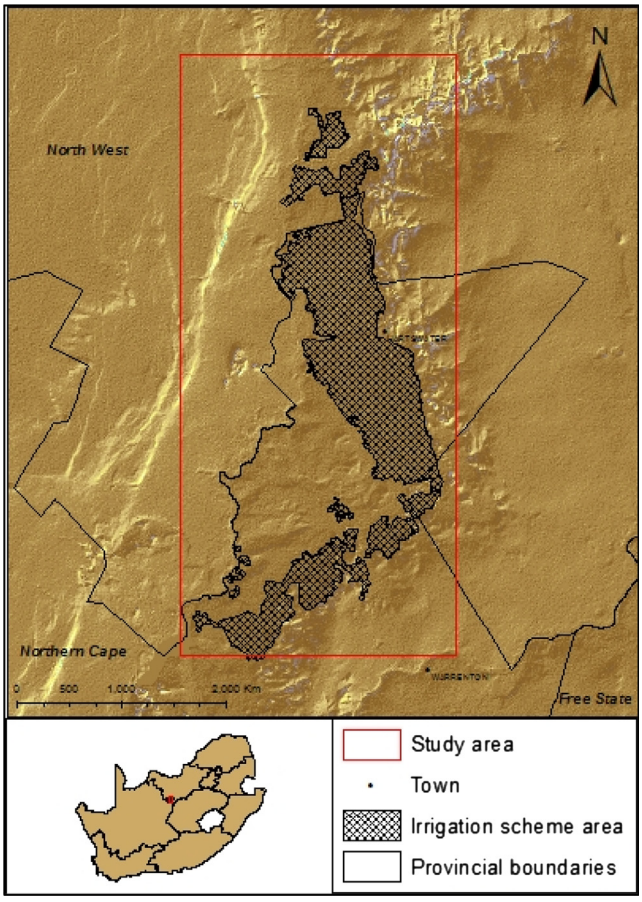

Fig. 1. Extent and location of the study area within South Africa.

2. Methods

2.1. Study area

The Vaalharts irrigation scheme (Fig. 1) is located at the border of the Northern Cape, North West and Free State provinces of South Africa, near the towns of Warrenton and Hartswater. The area is approximately 369.5 square kilometres in size and has a semi-arid climate with cold, dry winters and long warm summers (Maisela, 2007). The annual rainfall is approximately 450 mm, with around 89% of precipitation falling during summer (October–April), peaking from January to April (Maisela, 2007). The main crops grown in the area are maize, barley, groundnuts, pecan nuts and lucerne. Wheat, barley and lucerne are grown during the dry winter months.

2.2. Image collection

In this study, focus was placed on the summer growing season when the diversity of crops is at its greatest. Seven cloud-free Sentinel-2 images were acquired for the months of November 2016 to April 2017. The Sentinel-2 satellite constellation offers spatial resolutions of 10 m, 20 m and 60 m across 12 bands with a revisit time of five days (Table 1). The Sentinel-2 imagery was acquired in Level-1C format, which is radiometrically and geometrically corrected to top of atmosphere (TOA) reflectance.

2.3. Experimental overview

The OBIA experiments evaluated in this study consisted of five main processing steps:

Table 1
Details of the Sentinel-2 satellites characteristics including band names, wavelength and spatial resolution.

Sentinel-2 bands	Central wavelength (μm)	Resolution (m)
Band 1 – Coastal aerosol	0.443	60
Band 2 – Blue	0.490	10
Band 3 – Green	0.560	10
Band 4 – Red	0.665	10
Band 5 – Vegetation red edge	0.705	20
Band 6 – Vegetation red edge	0.740	20
Band 7 – Vegetation red edge	0.783	20
Band 8 – Near infrared (NIR)	0.842	10
Band 8A – Vegetation red edge	0.865	20
Band 9 – Water vapour	0.945	60
Band 10 – SWIR – cirrus	1.375	60
Band 11 – SWIR	1.610	20
Band 12 – SWIR	2.190	20

1. Edge detection, performed on all individual images;
2. Aggregation of edge layers generated in Step 1;
3. Image segmentation, carried out on the aggregated edge image produced in Step 2;
4. Discarding of uncultivated image objects; and
5. Removal of noise.

The following subsections expand on each of these steps.

2.3.1. Step 1: Edge detection

Two edge detection algorithms were considered in Step 1, namely the Scharr and Canny operators (Table 2). An edge in an image can be defined as a sharp change or discontinuity in the grey level values (Christe et al., 2011; Ramadevi et al., 2010; Rydberg & Borgefors, 2001; Shrivakshan & Chandrasekar, 2012). Edge detection is a very common operation performed in image analysis, and many algorithms have been developed for detecting and enhancing edges (Christe et al., 2011). Examples include Sobel, Prewitt, Robert, Scharr and Canny. The edge detection algorithm generates an edge layer, which can be described as a grey level image representing object edges. High grey level values indicate a sharp discontinuity with the adjacent pixels. The Canny and Scharr operators were used in this study due to their superior performance in comparison to other edge detection algorithms (Batra et al., 2016; Muthukrishnan & Radha, 2011; Sharma & Mahajan, 2017).

2.3.1.1. Canny edge detection. The Canny edge detector is generally considered to provide better results than other edge detectors and is often used as a benchmark against which other edge operators are compared (Canny, 1986). The Canny operator involves a multistage process that can be summarized as follows: the image is first smoothed with a Gaussian filter, followed by gradient computation, non-maxima suppression and hysteresis thresholding (Juneja & Sandhu, 2009). The Trimble eCognition Developer (version 9) implementation of the Canny algorithm was used in this study.

2.3.1.2. Scharr edge detection. The Scharr operator was developed to alleviate the rotational invariance inherent in operators such as Sobel

Table 2
Description of the different algorithm scenarios.

Scenario	Edge detection algorithm	Segmentation method
MTS_C	Canny	MTS
MTS_S	Scharr	MTS
MRS_C	Canny	MRS
MRS_S	Scharr	MRS
WS_C	Canny	WS
WS_S	Scharr	WS

G_x =

3	0	-3
10	0	-10
3	0	-3

G_y =

3	10	3
0	0	0
-3	-10	-3

Fig. 2. Horizontal and vertical Scharr edge masks.

and Prewitt (Kroon, 2009; Scharr, 2007). This is achieved by using differently weighted horizontal and vertical edge masks, as shown in Fig. 2. These edge masks help to suppress noise that is inherent in the Sobel operator (Christe et al., 2011).

The Scharr edge detection algorithm was implemented in Python using the Scikit-image library (version 0.13.1). The algorithm requires no input parameters, apart from the input image.

The Canny and Scharr algorithms were applied on all seven cloud-free Sentinel-2 images collected from November 2016 to April 2017. The red, blue, green and NIR bands were used as input to the edge detection algorithms due to their relatively high (10 m) spatial resolution. This resulted in four 10 m resolution edge layers per image per operator.

2.3.2. Step 2: Edge layer aggregation

Step 2 of the workflow involved the aggregation of the 28 (4 bands × 7 acquisition dates) multi-temporal edge layers generated by each edge operator. A simple equal weight summation of the edge layers was used to combine the images into one composite, multi-temporal edge image per operator.

2.3.3. Step 3: Image segmentation

In the image segmentation step (Step 3), the aggregated edge images (one for Canny and one for the Scharr operator) were used as input to three selected image segmentation algorithms, namely MRS, WS and MTS. The MRS and WS algorithms were chosen due to their frequent use in agricultural applications (Butenuth et al., 2004; Conrad et al., 2010; Lebourgeois et al., 2017; Li et al., 2010; Peña et al., 2014; Schultz et al., 2015). The MTS algorithm was selected as it is an effective technique to rapidly segment images based on the distribution of the input image's histogram (Carleer et al., 2005).

2.3.3.1. Watershed segmentation. WS is a region-based algorithm that is applied to a single gradient image (Li et al., 2010). The objective of the algorithm is to find the high gradient magnitudes (watersheds) that divide regions of local minima (basins) (Salman, 2006). The algorithm uses local minima as seed points and expands objects outward with rising intensity levels. Objects cease to expand after they reach the borders of another object. The WS algorithm is prone to over-segmentation and often produces a large number of small objects, thereby making it necessary to perform some form of region merging during or after the execution (Bleau & Leon, 2000).

The WS algorithm, as implemented in Trimble eCognition Developer 9, has four parameters for region merging, namely area, height, depth and volume. The height parameter is used to control when adjacent objects should be merged (i.e. when an object's maximum pixel value is below the specified height threshold). Given that the ultimate aim is to develop an automated system for field boundary delineation, Jenks' (Jenks, 1967) natural breaks (JNB) algorithm, as implemented in ArcMap (version 10.4.1), was used to automatically find a suitable threshold. The JNB algorithm minimises intra-class variance while maximising inter-class variance. The algorithm was used to sequentially group the pixel values into two, three, four and five classes to find the most suitable thresholds. Through experimentation it was determined that grouping pixels into three classes and using the threshold separating the first and second class produced the best merging threshold for the WS algorithm. The final threshold values were 0.1214 and 0.0812 for the Canny and Scharr edge layers respectively.

2.3.3.2. Multi-resolution segmentation. MRS, as implemented in Trimble eCognition Developer 9, is a region-based procedure that maximises the homogeneity within objects while minimising the average heterogeneity between objects (Baatz & Schäpe, 2000). The MRS procedure follows a mutual best fitting approach by starting with image objects of one pixel and repeatedly merging them based on a user-defined homogeneity criterion. MRS parameters were chosen using a trial and error approach where individual parameters were systematically increased and the resulting segmentations evaluated against reference field boundaries (see Section 2.4). The parameters that produced the most meaningful (slightly over-segmented) segmentation results were 60 (scale), 0.8 (compactness) and 0.5 (shape).

2.3.3.3. Multi-threshold segmentation. MTS classifies an image into subsets based on pre-defined threshold values (Trimble, 2016). For example, a single threshold will group the image pixels into two classes. The first class contains pixels with values below the defined threshold, while the second class contains pixels with values above the threshold. MTS was used in this study to group pixels into two classes, namely edge and not-edge. The edge pixels were then discarded, leaving only homogenous areas (objects) such as fields. The threshold values for the Canny and Scharr edge layers were identical to the WS thresholds (0.1214 and 0.0812 respectively).

2.3.4. Step 4: Uncultivated area exclusion

Expert rules were used in Step 4 to automatically discard uncultivated areas from further consideration. The rule-set was designed to be reproducible and fully automatic. Normalised difference vegetation index (NDVI) time series have been shown to correlate strongly with the phenology of crops during the growing season (Huete, 1988; Maselli & Rembold, 2001; Zheng et al., 2015). Four NDVI-based features, namely maximum, minimum, range and standard deviation were consequently extracted per pixel from the seven Sentinel-2 images considered. These features were used as input to a classification and regression tree (CART) algorithm to generate a decision tree for separating (classifying) cultivated and uncultivated objects. Manually selected sample points were used to train the CART algorithm. The resulting rule-set was implemented in Trimble eCognition Developer (version 9) software and used in all experiments. An additional threshold-based rule was added to the MRS workflow to remove sliver polygons (i.e. high magnitude edges) along the field boundaries that were erroneously classified by the decision tree as crop fields. The rule makes use of the Scharr and Canny edge layers to identify and discard objects (segments) with high edge values. The threshold values for the Scharr (0.0812) and Canny (0.1214) edge layers that were determined using the JNB algorithm and applied to the WS and MTS implementations were used for this purpose.

2.3.5. Step 5: Noise removal

Although OBIA approaches are not prone to the so-called "salt-and-pepper" effect of per-pixel classifications, noisy imagery can cause the formation of small (< 40 pixels) objects during segmentation. In this study, some small objects related to infrastructure (e.g. pivot irrigation) or small areas affected by soil conditions (e.g. salt accumulation and waterlogging) were present in some of the fields. A simple rule to identify and discard small objects that were completely surrounded by cultivated areas was used in the final step (Step 4) of the workflow to remove such anomalies.

2.4. Accuracy assessment

A reference field boundary dataset, consisting of 400 fields, was manually digitised from very high resolution (10 cm) aerial imagery acquired in February and March 2016. Given that the aerial imagery was captured a year prior to the Sentinel-2 imagery used in the

experiments, the digitised field boundaries were overlaid onto red, green and blue composites of the Sentinel-2 images acquired in the 2016–2017 growing season to remove inconsistent reference boundaries (i.e. boundaries that changed between March 2016 and the 2016–2017 growing season were discarded from the reference field boundary dataset).

Despite the popularity of image segmentation algorithms, effective and efficient methods to evaluate the ability of a segmentation algorithm to accurately delineate boundaries of the objects of interest remain elusive (Clinton et al., 2010; Meyer & Van Niekerk, 2015). Over-segmentation (OS), under-segmentation (US) and boundary offset are the most common causes of poor or inappropriate image segmentations, and no single accuracy measure can sufficiently quantify all of these errors in combination (Weidner, 2008). OS and US is commonly measured using topological (area) relationships, while boundary offsets are calculated using geometrical (edge) metrics (Zhan et al., 2005). Several area-based metrics have been proposed to calculate OS and US (Clinton et al., 2010; Möller et al., 2007; Weidner, 2008), but these measures do not take the accuracy of delineated boundaries into account. A common edge metric, such as proposed by Delves et al. (1992), calculates the average distance error between reference and extracted object boundaries and has proven to be successful in determining the accuracy of segmented boundaries (Meyer & Van Niekerk, 2015). A similar edge metric, namely the mean absolute error (MAE) distance metric, was implemented in this study.

MAE considers the Euclidean distance (ED) between the centres of two cells representing the reference and extracted boundary respectively (Fig. 3). Two different instances of MAE were calculated to evaluate how closely the extracted field boundaries matched those in the reference database. MAE_i measures the distance from each reference boundary cell to the nearest extracted boundary cell, which provides an indication of how close in geographical space the extracted boundaries are to the actual boundary. Conversely, MAE_j measures the distance from each extracted boundary cell to the nearest reference boundary cells and is an indicator of boundaries within a field (caused by OS). The formulae to calculate both instances of MAE are defined as:

$$MAE_i = \frac{\sum EDi}{N} \quad (1)$$

where ED_i refers to the ED measured from the centre of the reference cell to the centre of the extracted cell, while N is the total number of boundary cells in the reference dataset.

$$MAE_j = \frac{\sum EDj}{N} \quad (2)$$

where ED_j refers to the ED measured from the centre of the extracted cell to the centre of the reference cell. MAE_i and MAE_j were summed to get a sense of overall agreement between the reference boundaries and those that were extracted, with low values indicating a high agreement.

$$MAE = MAE_i + MAE_j \quad (3)$$

The blue arrows in Fig. 3b illustrate the increased distance calculated from the extracted field boundaries to the reference boundaries when OS occurs.

A confusion matrix was used to calculate several area-based metrics. The matrix consisted of 10,000 samples, with 5000 “boundary” samples selected randomly within 10 m of the reference boundaries and another 5000 “not-boundary” samples randomly selected more than 10 m away from the reference boundaries. The accuracy metrics obtained from the confusion matrix included the overall accuracy (OA), Kappa index (K), commission error (CE) and omission error (OE). The OE provides an indication of extracted boundaries accuracy along the reference field boundaries, where a high error suggests that the segmentation did not delineate the field boundaries well. CE gives an indication of false boundaries within a field, often caused by OS within the fields. Additionally, the McNemar’s test was used to test for statistical significance, with p-values of 0.05 (or lower) taken as being significant.

3. Results

The results in Table 3 shows that the combination of WS and the Canny edge detection algorithm (experiment WS_C) produce the best OA (92.9%). This OA is, however, not significantly higher than the OA (92.7%) when the Scharr algorithm was combined with WS (i.e. experiment WS_S). In contrast, the OAs of these two experiments (WS_C and WS_S) are significantly higher ($p = 0.0001$) than the third best combination of algorithms, namely experiment MRS_C (80.5%). The lowest OA (70.3%) for any experiment was recorded for the MRS and Scharr combinations (MRS_S). Although the OA of MTS_S (71.9%) is only 1.6% higher than MRS_S, the McNemar’s test show a significant difference ($p = 0.0001$) between these two results. When the OEs are considered, the two WS experiments (WS_C and WS_S) performed on par with one another, with OEs ranging from 10.1% to 12.8%. In contrast, the OEs for the MTS and MRS experiments are significantly higher than the WS-based techniques and range from 35.6% to 54.9%. This clearly demonstrates that the WS-based techniques identify field boundaries much more accurately than the experiments involving MRS and MTS. Regarding CE, the WS_S experiment produced the lowest error (1.8%), and the highest CE was recorded by MTS_C (8.5%). The consistent superior performance of the WS-based experiments is underscored by the significantly ($p < 0.0001$) higher mean OA of 92.8%, compared to the mean OAs of 73.4% and 75.4% of the MTS and MRS respectively.

In contrast to the area-based metrics that show the WS_S and WS_C experiments to be on par with each other, the edge-based metrics reveal that the field boundaries of the WS_C experiments match the reference boundaries more closely than those of the WS_S experiment. Specifically, the MAE_i of the WS_C experiment is 7.6 m, which is significantly ($p = 0.0028$) lower than any of the other techniques

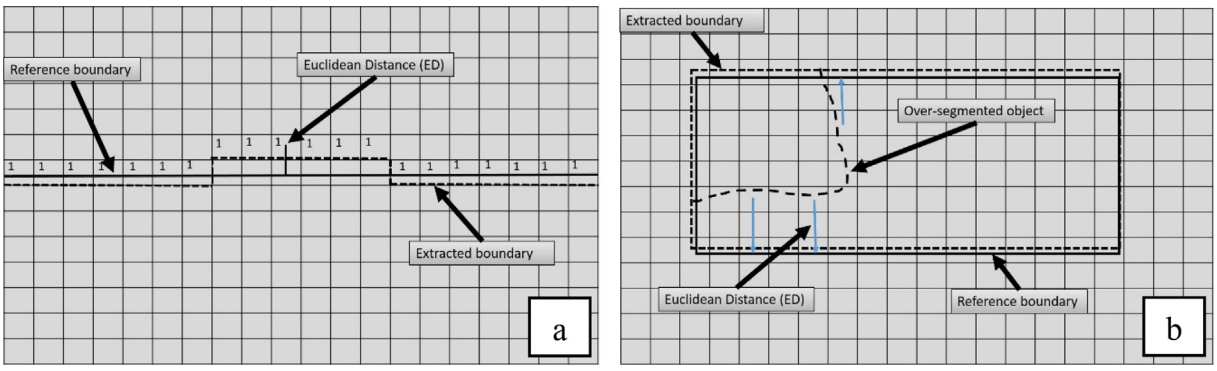

Fig. 3. Conceptual illustration of ED calculations, where (a) MAE_i is depicting the accuracy along the boundary and (b) MAE_j represents the level of OS.

Table 3
Area- and edge-based metric results for the six experiments.

	Area-based metrics					Edge-based metrics			
Experiment name	OA %	OE %	CE %	K	Mean OA %	MAE_i (m)	MAE_j (m)	Combined MAE	Mean combined MAE
MTS_C	74.8	41.9	8.5	0.5	73.4	15.2	28.3	33.5	35.5
MTS_S	71.9	51.9	4.3	0.44		17.9	19.5	37.4	
MRS_C	80.5	35.6	3.5	0.61	75.4	15.1	19.2	34.3	40.1
MRS_S	70.3	54.9	4.4	0.41		22.9	22.9	45.8	
WS_C	92.9	10.1	4.1	0.86	92.8	7.6	16.9	24.5	26.1
WS_S	92.7	12.8	1.8	0.9		16.5	11.3	27.8	

evaluated, including WS_S. The MAE_i of 7.6 m is remarkable as it means that the technique generated boundaries that are, on average, less than one pixel (10 m) displaced from the reference boundaries. This low MAE_i, however, came at the cost of a slightly elevated (16.9 m) MAE_j compared to the 11.3 m MAE_j of the WS_S experiment, which suggests that the level of OS is higher in WS_C compared to WS_S. Nevertheless, when the combined MAE of these two methods are compared, it seems that WS_C was substantially more accurate. Similarly, based on the edge metrics, the WS_C approach significantly outperformed the other edge and segmentation algorithm combinations.

Fig. 4 demonstrates the compositing of edge images. The edge layer for each individual date is the aggregation of four edge layers, generated from the red, green, blue and NIR bands. This example qualitatively illustrates how multi-temporal compositing of edge layers captures and accentuates persistent field boundaries. Some field boundaries that are faint (have low intensities) on specific dates become more pronounced as images of different dates are combined. One can also see that the Scharr algorithm tends to be more sensitive to variations (noise) within fields, which might have contributed to the WS_C experiment's superior accuracies.

Fig. 5 visualises the outputs of the six experiments in a small test site. Gaps between adjacent fields are clearly noticeable in the MTS and MRS approaches (Fig. 5c–f). These gaps represent edge objects that were removed in Step 4. Effectively, these edge objects offset the resulting boundaries by approximately one to three pixels towards the centre of the fields. This had a substantial effect on both the area and edge-based measures in Table 3.

4. Discussion

Both the area- and edge-based metrics show that the WS workflows significantly outperform those involving MRS and MTS. Although no other studies have directly compared the WS, MRS and MTS algorithms for field boundary delineation, Gaetano et al. (2015) found that a marker-based WS algorithm generated more accurate image objects than MRS using a 1 m resolution IKONOS image as input. However, this disagrees with Kavzoglu & Tonbul (2017) who found that MRS outperformed WS when using a 2 m resolution Worldview-2 image. A likely explanation for the improved performance of WS in our study is the multi-temporal approach used. Employing multi-temporal imagery reinforces object edges (in this case field boundaries), while potentially reducing the noise within a field as noise is unlikely to be present in the same location over multiple dates (as illustrated in Fig. 4). In addition, the WS method created sharper boundaries along the high magnitude edges, which resulted in more defined object borders. This is a conceptual difference between WS and the other segmentation techniques evaluated. WS attempts to create boundaries where the values are highest (i.e. at points of discontinuity), while MRS groups values together based on their homogeneity. High values (edges) are consequently often grouped together, which results in objects being formed along the boundaries of image features, in our case crop fields. The edge objects formed along the boundary cause the field edges to be shifted towards the centre, resulting in an offset between the reference and segmented field boundaries. This is evident in the lower accuracies obtained by the MRS and MTS workflows. It is likely that the MRS and MTS approaches can be improved by implementing additional rules

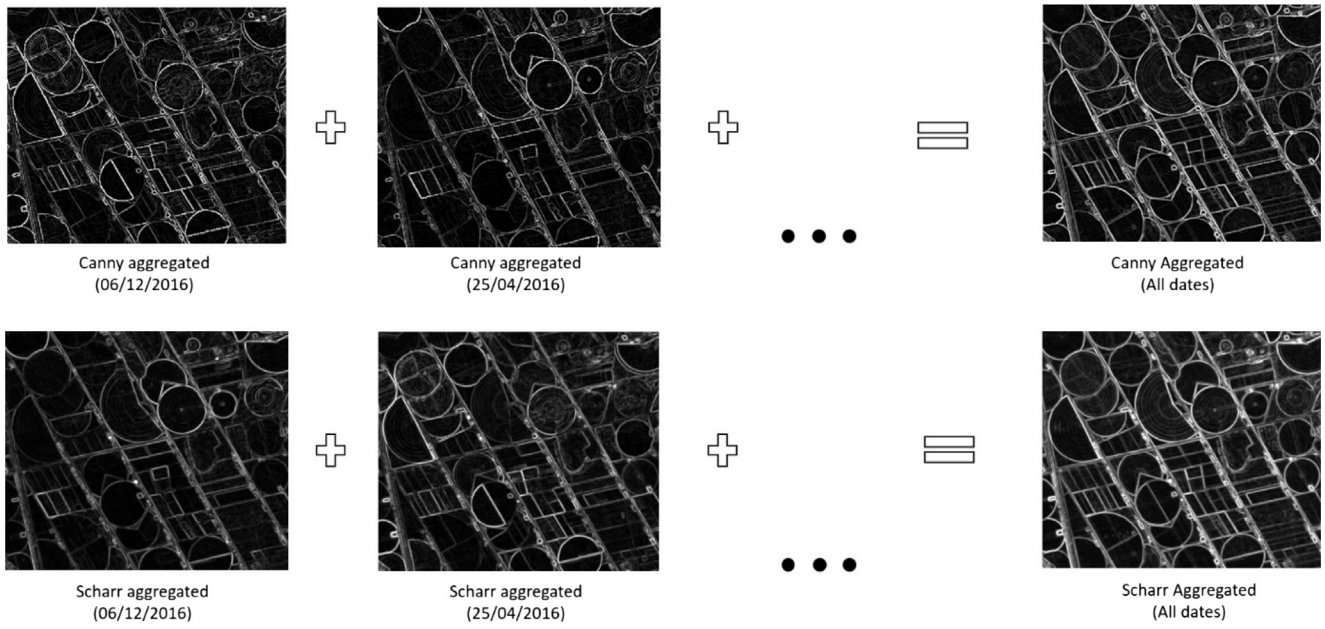

Fig. 4. Illustration of how the aggregation of multiple edge layers for the Canny and Scharr edge operators reinforce persistent edges.

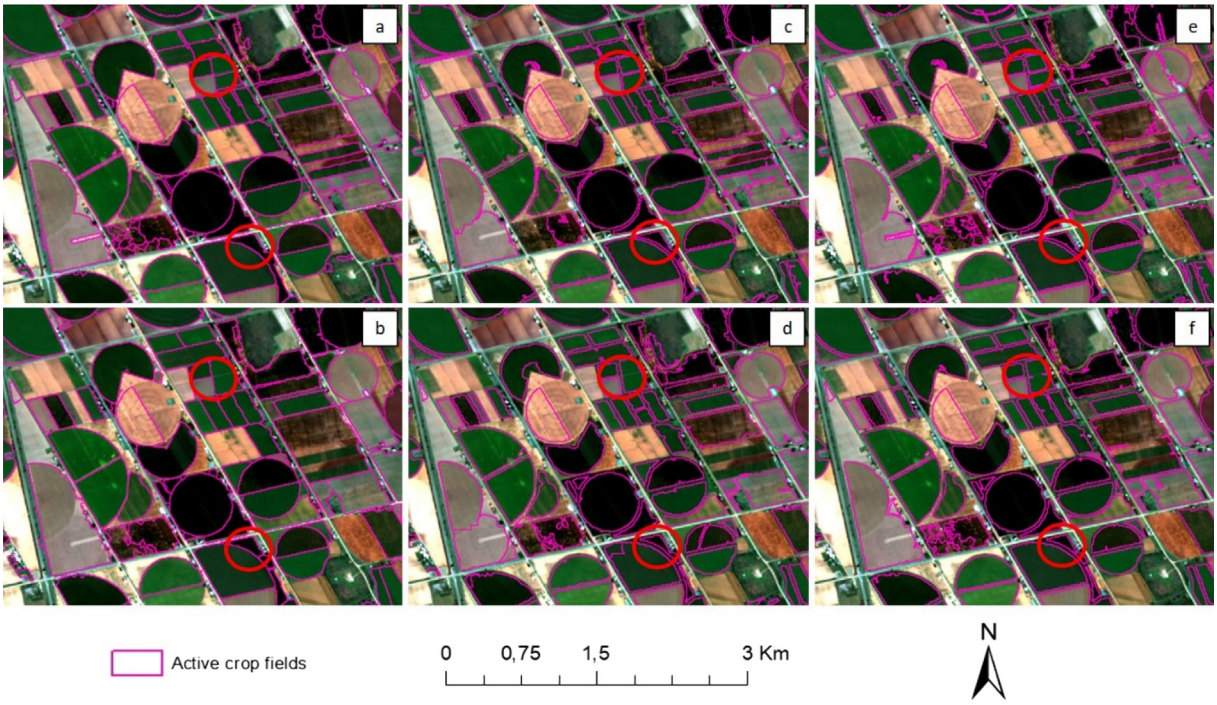

Fig. 5. Detailed area showing the field boundaries extracted by experiments (a) WS_C, (b) WS_S, (c) MRS_C, (d) MRS_S, (e) MTS_C and (f) MTS_S.

(e.g. object thinning or centre line extraction), but this will substantially increase the complexity of the workflow, which will likely reduce its robustness. Given the excellent performance and suitability of WS for the task at hand, an attempt to add rules to improve the MRS and MTS results seemed pointless (especially within the context of finding a technique that can be operationalised). However, it is acknowledged that the MRS and MTS may perform better with such rules.

The results obtained from the area- and edge-based metrics show that the WS_C experiment provides far more accurate and consistent results than the WS_S experiment, thus illustrating the superior performance of the Canny edge detection algorithm. This is consistent with findings of Juneja & Sandhu (2009) and Maini & Aggarwal (2009) who also found that the Canny edge detector produces better overall results. A likely explanation is the improved signal to noise ratio established by the non-maxima suppression method used by the Canny operator (Shrivakshan & Chandrasekar, 2012). The non-maxima suppression results in magnitude edges with a width of one pixel, which allows WS to more accurately delineate the boundaries. In contrast, the Scharr algorithm does not use non-maxima suppression and thus creates thicker edges, which can cause uncertainties and reduce the WS's ability to find sharp boundaries (i.e. the boundaries become erratic). The slightly higher OS observed for the Canny edge detector (Table 3) agrees with Batra et al. (2016), who showed that the improved capability of the Canny algorithm to detect weak edges can cause the generation of false edges within fields, which in turn leads to too many objects being created during segmentation.

Our results show that multi-temporal Sentinel-2 imagery holds much potential for delineating field boundaries. The 10 m spatial resolution of the Sentinel-2 images seems sufficient in most cases, although not ideal for small and narrow fields. Similar observations were made by Lebourgeois et al. (2017) who used Landsat-8 and SPOT-5 imagery to simulate Sentinel-2 time series imagery for mapping smallholder fields. They found that the spatial resolution of Sentinel-2 is potentially too low to map some of the smaller and irregularly-shaped fields. Although the spectral resolution of Sentinel-2 imagery is higher than those of many other EO satellites (e.g. Landsat-8, SPOT-6/7, RapidEye), only four of the bands are at 10 m resolutions. The other bands, such as red edge and SWIR bands, will likely improve discrimination between agricultural land covers, but owing to their relatively low (20–60 m) spatial resolutions, they have little value for field boundary delineations (Valero et al., 2016). Despite these shortcomings, the boundaries produced in this study were generally highly accurate. This is mainly attributed to the use of a time series of images in the edge detection process, as illustrated in Fig. 4. Although the increased temporal frequency of Sentinel-2 imagery has significant advantages, the selection of cloud free imagery is critical. A limitation of this study was the manual selection of cloud-free imagery. However, image compositing techniques such as rule-based compositing and linear temporal resampling have been proposed as possible solutions for creating cloudless and artefact-free imagery (Inglada et al., 2015; Lück & Van Niekerk, 2016).

A wide range of annual crops are grown in Vaalharts and as such it was an ideal testing site. However, it is unclear whether the recommended WS_C method will perform equally well in other agricultural areas and under different conditions. For instance, the phenology of perennial crops (e.g. vineyards and fruit trees) grown in the Mediterranean climate of the Western Cape Province are very different to the annuals grown in Vaalharts. More work is therefore needed to investigate the transferability and robustness of the methods evaluated in this study. Given their demonstrated superiority, future efforts should focus on the WS-based methods.

5. Conclusion

This study compared and evaluated six multi-temporal OBIA approaches for identifying and delineating active crop field boundaries. The approach combined two edge enhancement (Canny and Scharr) and three image segmentation (WS, MRS and MTS) techniques. The key findings and conclusions of the study are:

1. Canny edge detection provides finer field boundary edges compared to the Scharr algorithm and is consequently better suited for enhancing field boundaries.
2. WS is more suitable than MRS and MTS for delineating agricultural field boundaries when edge layers are used as input to the algorithms.

3. The relatively low spatial resolution of Sentinel-2 imagery limits the delineation of small, narrow or irregularly-shaped fields, but was sufficient for the majority of fields in the study area.
4. Due to the dynamic nature of field crops (especially annuals), a multi-temporal approach to field boundary delineation is essential.
5. More work is needed to evaluate the Canny edge detection and WS segmentation approach in other agricultural environments.

Given the results obtained in this study, the Canny edge detection algorithm, in conjunction with WS, is effective in a multi-temporal approach to delineate active crop fields. The WS experiments show good potential for use in an operational workflow, although future research should focus on applying it on a regional or national scale. Nevertheless, the high accuracy suggests that the WS workflow can provide valuable information about the extent and location of agricultural field boundaries. These boundaries can be subsequently used in agricultural monitoring systems to aid the implementation of precision agriculture, crop yield estimations, food security assessments and resource planning.

Acknowledgements

This work forms part of a larger project titled “Salt Accumulation and Waterlogging Monitoring System (SAWMS) Development” which was initiated and funded by the Water Research Commission (WRC) of South Africa (contract number K5/2558//4). More information about this project is available in the 2016/2017 WRC Knowledge Review (ISBN 978-1-4312-0912-5) available at www.wrc.org.za. The authors would also like to thank the Centre for Geographical Analysis for providing the Sentinel-2 data, and the National Research Foundation (grant number 106739) for their funding of this project.

References

Alemu, M.M., 2016. Automated farm field delineation and crop row detection from satellite images. [online]. Available from:. University of Twente. http://www.itc.nl/library/papers_2016/msc/gfm/alemu.pdf.

Baatz, M., Schäpe, A., 2000. Multiresolution Segmentation: an optimization approach for high quality multi-scale image segmentation. [online]. Available from: In: Angewandte Geographische Informationsverarbeitung XII. Beiträge zum AGIT-Symposium Salzburg 2000, Karlsruhe, Herbert Wichmann Verlag, pp. 12–23. http://scholar.google.com/scholar?hl=en&btnG=Search&q=intitle:Multiresolution+Segmentation+:+an+optimization+approach+for+high+quality+multi-scale+image+segmentation#1.

Batra, B., Singh, S., Sharma, J., Arora, S.M., 2016. Computational analysis of edge detection operators. Int. J. Appl. Res. 2 (11), 257–262.

Belgiu, Mariana, Csillik, Ovidiu, 2018. Sentinel-2 cropland mapping using pixel-based and object-based time-weighted dynamic time warping analysis. Rem. Sens. Environ. 204, 509–523. https://doi.org/10.1016/j.rse.2017.10.005.

Blaschke, T., Hay, G.J., Kelly, M., Lang, S., Hofmann, P., Addink, E., Queiroz Feitosa, R., van der Meer, F., van der Werff, H., van Coillie, F., Tiede, D., 2014. Geographic object-based image analysis – towards a new paradigm. ISPRS J. Photogramm. Rem. Sens. 87, 180–191. https://doi.org/10.1016/j.isprsjprs.2013.09.014.

Bleau, A., Leon, L.J., 2000. Watershed-based segmentation and region merging. Available from:. Comput. Vis. Image Underst. 77, 317–370. http://www.sciencedirect.com/science/article/pii/S1077314299908226.

Bontemps, S., Arias, M., Cara, C., Dedieu, G., Guzzonato, E., Hagolle, O., Inglada, J., Matton, N., Morin, D., Popescu, R., Rabaute, T., Savinaud, M., Sepulcre, G., Valero, S., Ahmad, I., Bégué, A., Wu, B., de Abelleyra, D., Diarra, A., Dupuy, S., French, A., Akhtar, I.ul H., Kussul, N., Lebourgeois, V., Page, M. Le, Newby, T., Savin, I., Verón, S.R., Koetz, B., Defourny, P., 2015. Building a data set over 12 globally distributed sites to support the development of agriculture monitoring applications with Sentinel-2. Rem. Sens. 7 (12), 16062–16090.

Butenuth, M., Straub, B., Heipke, C., 2004. Automatic extraction of field boundaries from aerial imagery. In: KDNet Symposium on Knowledge-Based Services for the Public Sector, pp. 14–25.

Canny, J., 1986. A computational approach to edge detection. IEEE Trans. Pattern Anal. Mach. Intell. PAMI-8 (6), 679–698.

Carleer, A.P., Debeir, O., Wolff, E., 2005. Assessment of very high spatial resolution satellite image segmentations. [online]. Available from:. Photogramm. Eng. Rem. Sens. 71 (11), 1285–1294. http://www.armurs.ulb.ac.be/images/8/86/PERS_Carleer_05.pdf.

Chen, B., Qiu, F., Wu, B., Du, H., 2015. Image segmentation based on constrained spectral variance difference and edge penalty. Rem. Sens. 7 (5), 5980–6004.

Christe, M.S.A., Vignesh, M., Kandaswamy, A., 2011. an Efficient Fpga Implementation of Mri Image Filtering and Tumour Characterization Using Xilinx System Generator. Int. J. VLSI Des. Commun. Syst. (VLSICS) 2 (4), 95–109.

Clinton, N., Holt, A., Scarborough, J., Yan, L., Gong, P., 2010. Accuracy assessment measures for object-based image segmentation goodness. Photogramm. Eng. Rem. Sens. 76 (3), 289–299.

Conrad, C., Fritsch, S., Zeidler, J., Rücker, G., Dech, S., 2010. Per-field irrigated crop classification in arid Central Asia using SPOT and ASTER data. Rem. Sens. 2 (4), 1035–1056.

Delves, L., Wilkinson, R., Oliver, C., White, R., 1992. Comparing the performance of SAR image segmentation algorithms. Int. J. Rem. Sens. 13 (11), 2121–2149.

Drusch, M., Del Bello, U., Carlier, S., Colin, O., Fernandez, V., Gascon, F., Hoersch, B., Isola, C., Laberinti, P., Martimort, P., Meygret, A., Spoto, F., Sy, O., Marchese, F., Bargellini, P., 2012. Sentinel-2: ESA’s optical high-resolution mission for GMES operational services. Rem. Sens. Environ. 120, 25–36.

Esfahani, A.L.I.G., 2014. Delineation of Agricultural Field Boundaries Using Random Sets. University of Twente.

Fan, J., Yau, D.K.Y., Elmagarmid, A.K., Aref, W.G., 2001. Automatic image segmentation by integrating color-edge extraction and seeded region growing. IEEE Trans. Image Process. 10 (10), 1454–1466.

Gaetano, R., Masi, G., Poggi, G., Verdoliva, L., Scarpa, G., 2015. Marker-controlled watershed-based segmentation of multiresolution remote sensing images. IEEE Trans. Geosci. Rem. Sens. 53 (6), 2987–3004.

Gilbertson, Jason Kane, Kemp, Jaco, van Niekerk, Adriaan, 2017. Effect of pan-sharpening multi-temporal Landsat 8 imagery for crop type differentiation using different classification techniques. Comput. Electron. Agric. 134, 151–159. https://doi.org/10.1016/j.compag.2016.12.006.

Huete, A.R., 1988. A soil-adjusted vegetation index (SAVI). Rem. Sens. Environ. 25 (3), 295–309.

Inglada, J., Arias, M., Tardy, B., Hagolle, O., Valero, S., Morin, D., Dedieu, G., Sepulcre, G., Bontemps, S., Defourny, P., Koetz, B., 2015. Assessment of an operational system for crop type map production using high temporal and spatial resolution satellite optical imagery. Rem. Sens. 7 (9), 12356–12379.

Jenks, G.F., 1967. International Yearbook of Cartography, seventh ed.

Johnson, David M., 2013. A 2010 map estimate of annually tilled cropland within the conterminous United States. Agric. Syst. 114, 95–105. https://doi.org/10.1016/j.agsy.2012.08.004.

Juneja, M., Sandhu, P.S., 2009. Performance evaluation of edge detection techniques for images in spatial domain. Int. J. Comput. Theory Eng. 1 (5), 614–622.

Kavzoglu, T., Tonbul, H., 2017. A comparative study of segmentation quality for multi-resolution segmentation and watershed transform. IEEE. 2, June.

Kroon, D.-J., 2009. Numerical optimization of kernel based image derivatives Dirk-Jan Kroon University of Twente, Enschede. December. [online]. Available from:. http://www.k-zone.nl/Kroon_DerivativePaper.pdf.

Lebourgeois, V., Dupuy, S., Vintrou, É., Ameline, M., Butler, S., Bégué, A., 2017. A combined random forest and OBIA classification scheme for mapping smallholder agriculture at different nomenclature levels using multisource data (simulated Sentinel-2 time series, VHRS and DEM). Rem. Sens. 9 (3), 1–20.

Li, D., Zhang, G., Wu, Z., Yi, L., 2010. An edge embedded marker-based watershed algorithm for high spatial resolution remote sensing image segmentation. IEEE Trans. Image Process. 19 (10), 2781–2787.

Lück, W., van Niekerk, A., 2016. Evaluation of a rule-based compositing technique for Landsat-5 TM and Landsat-7 ETM+ images. Int. J. Appl. Earth Obs. Geoinform. 47, 1–14. https://doi.org/10.1016/j.jag.2015.11.019.

Lunetta, Ross S., Shao, Yang, Ediriwickrema, Jayantha, Lyon, John G., 2010. Monitoring agricultural cropping patterns across the Laurentian Great Lakes Basin using MODIS-NDVI data. Int. J. Appl. Earth Obs. Geoinform. 12 (2), 81–88. https://doi.org/10.1016/j.jag.2009.11.005.

Maini, R., Aggarwal, H., 2009. Study and comparison of various image edge detection techniques. Int. J. Image Process. 3 (1), 1–11.

Maisela, R.J., 2007. Realizing agricultural potential in Land Reform: the case of Vaalharts irrigation scheme in the Northern Cape Province. University of the Western Cape.

Maselli, F., Rembold, F., 2001. In: Analysis of GAC NDVI Data for Cropland Identification and Yield Forecasting in Mediterranean African Countries, May, pp. 593–602.

Meyer, H.P., Van, Niekerk A., 2015. Assessing Edge and Area Metrics for Image Segmentation Parameter Tuning and Evaluation.

Möller, M., Lymburner, L., Volk, M., 2007. The comparison index: a tool for assessing the accuracy of image segmentation. Int. J. Appl. Earth Obs. Geoinform. 9 (3), 311–321.

Mueller, M., Segl, K., Kaufmann, H., 2004. Edge- and region-based segmentation technique for the extraction of large, man-made objects in high-resolution satellite imagery. Pattern Recogn. 37 (8), 1619–1628.

Muthukrishnan, R., Radha, M., 2011. Edge detection techniques for image segmentation. [online]. Available from:. Int. J. Comput. Sci. 3 (6), 259–267. http://scholar.google.com/scholar?hl=en&btnG=Search&q=intitle:EDGE+DETECTION+TECHNIQUES+FOR+image+segmentation#0.

Peña, J., Gutiérrez, P., Hervás-Martínez, C., Six, J., Plant, R., López-Granados, F., 2014. Object-based image classification of summer crops with machine learning methods. [online]. Available from. Rem. Sens. 6 (6), 5019–5041. http://www.mdpi.com/2072-4292/6/6/5019/.

Pittman, K., Hansen, M.C., Becker-Reshef, I., Potapov, P.V., Justice, C.O., 2010. Estimating global cropland extent with multi-year MODIS data. Rem. Sens. 2 (7), 1844–1863.

Ramadevi, Y., Sridevi, T., Poornima, B., Kalyani, B., 2010. Segmentation and object recognition using edge detection techniques. Int. J. Comput. Sci. Inform. Technol. 2 (6), 153–161.

Roumenina, E., Atzberger, C., Vassilev, V., Dimitrov, P., Kamenova, I., Banov, M., Filchev, L., Jelev, G., 2015. Single- and multi-date crop identification using PROBA-V 100 and

300 m S1 products on Zlatia Test Site, Bulgaria. Rem. Sens. 7 (10), 13843–13862.
Rydberg, A., Borgefors, G., 2001. Integrated method for boundary delineation of agricultural fieldsin multispectral satellite images. IEEE Trans. Geosci. Rem. Sens. 39 (11), 1678–1680.
Rydberg, A., Borgefors, G., 1999. Extracting multispectral edges in satellite images over agricultural fields. In: Proceedings - International Conference on Image Analysis and Processing, ICIAP, pp. 786–791.
Salman, N., 2006. Image segmentation based on watershed and edge detection techniques. Int. Arab J. Inform. Technol. 3 (2), 104–110.
Scharr, H., 2007. Optimal filters for extended optical flow. [online]. Available from: In: ResearchGate, pp. 91–103. http://www.springerlink.com/index/F561031610812Q7U.pdf.
Schultz, B., Immitzer, M., Formaggio, A.R., Sanches, I.D.A., Luiz, A.J.B., Atzberger, C., 2015. Self-guided segmentation and classification of multi-temporal Landsat 8 images for crop type mapping in Southeastern Brazil. Rem. Sens. 7 (11), 14482–14508.
Sharma, S., Mahajan, V., 2017. Study and analysis of edge detection techniques in digital images. IJSRSET 3 (5), 328–335.
Shrivakshan, G.T., Chandrasekar, C., 2012. A comparison of various edge detection techniques used in image processing. [online]. Available from:. Int. J. Comput. Sci. Iss. (IJCSI) 9 (5), 269–276. http://ul.summon.serialssolutions.com/2.0.0/link/0/.
Trimble, 2016. eCognition ® Developer 9.2.eCognition ® Developer 9.2.
Turker, Mustafa, Kok, Emre Hamit, 2013. Field-based sub-boundary extraction from remote sensing imagery using perceptual grouping. ISPRS J. Photogramm. Rem. Sens. 79, 106–121. https://doi.org/10.1016/j.isprsjprs.2013.02.009.
Valero, S., Morin, D., Inglada, J., Sepulcre, G., Arias, M., Hagolle, O., Dedieu, G., Bontemps, S., Defourny, P., Koetz, B., 2016. Production of a dynamic cropland mask by processing remote sensing image series at high temporal and spatial resolutions. Rem. Sens. 8 (1), 1–21.
Wardlow, B.D., Egbert, S.L., Kastens, J.H., 2007. Analysis of time-series MODIS 250m vegetation index data for crop classification in the U.S. Central Great Plains. Rem. Sens. Environ. 108, 3, 290–310.
Weidner, U., 2008. Contribution to the assessment of segmentation quality for remote sensing applications. Int. Arch. Photogramm. Rem. Sens. Spatial Inform. Sci. 37 (B7), 479–484.
Wuest, Ben, Zhang, Yun, 2009. Region based segmentation of QuickBird multispectral imagery through band ratios and fuzzy comparison. ISPRS J. Photogramm. Rem. Sens. 64 (1), 55–64. https://doi.org/10.1016/j.isprsjprs.2008.06.005.
Yan, L., Roy, D.P., 2014. Automated crop field extraction from multi-temporal Web Enabled Landsat Data. Rem. Sens. Environ. 144, 42–64. https://doi.org/10.1016/j.rse.2014.01.006.
Zhan, Q., Molenaar, M., Tempfli, K., Shi, W., 2005. Quality assessment for geo-spatial objects derived from remotely sensed data. Int. J. Rem. Sens. 26 (14), 2953–2974.
Zheng, Baojuan, Myint, Soe W., Thenkabail, Prasad S., Aggarwal, Rimjhim M., 2015. A support vector machine to identify irrigated crop types using time-series Landsat NDVI data. Int. J. Appl. Earth Obs. Geoinform. 34, 103–112. https://doi.org/10.1016/j.jag.2014.07.002.